Supplemental Data to**:**

Pharmacokinetics and Disposition of Momelotinib Revealed a Disproportionate Human Metabolite – Resolution for Clinical Development

Jim Zheng, Yan Xin, Jingyu Zhang, Raju Subramanian, Bernard P. Murray, J. Andrew Whitney, Matthew R. Warr, John Ling, Lisa Moorehead, Ellen Kwan, Jeffrey Hemenway, Bill J. Smith, Jeffrey A. Silverman

Drug Metabolism and Disposition

Supplemental Materials and Methods

Human Single-Dose mass balance study: metabolic profiling methodology

Metabolite profiling and identification were performed on a HPLC coupled to radioactivity and MS detectors. The integrated system consisted of Agilent 1100 HPLC with quaternary pumps, autosampler, diode array UV detector, LTQ Orbitrap mass spectrometer (Thermo Scientific, San Jose, CA) and a Perkin Elmer 625TR radioactivity flow detector. The radioactivity flow detector, Flow-one, equipped with a 100 µL flow cell, was operated using scintillation cocktail (Ultima Flo M) delivered at flow rate of 1.5 mL/min. Chromatography was accomplished on a Kinetic C18 column, 150 x 4.6 mm, 2.6 µm (Phenomenex, Torrance, CA), maintained at ambient temperature. Mobile phase A (MPA) was 10 mM ammonium acetate (NH_4AC) in water (pH 5.0), and mobile phase B (MPB) was 100% acetonitrile (ACN). The LC gradient is shown below:

Time (min)	MPA	MPB	Flow Rate (µL/min)
0	96	4	600
2	96	4	600
2.2	85	15	600
30	70	30	600
35	55	45	600

35.2	0	100	600
40	0	100	600
40.2	96	4	600
50	96	4	600

The first 5 minutes of the HPLC flow was diverted to the waste. Thermo Finnigan LTQ Orbitrap mass spectrometer (Thermo Scientific, San Jose, CA) was equipped with an electrospray ionization (ESI) interface and operated in positive ionization mode for metabolite profiling and identification. Mass spectra (Supplemental Figure S1 to S10) were acquired in full scan (MS) (*m/z* 150-1500) and data dependent scan (MS^2, MS^3, and MS^4) modes with CID activation method. Mass spectra were processed with the option of one decimal point for m/z with the measured accurate mass showing four decimal points reported in Supplemental Table S2. The parameters for the LTQ mass spectrometer used for the analysis are: spray voltage: +5.0 kV; capillary temperature: 300°C; sheath gas: 80 (arbitrary unit); auxiliary gas: 20 (arbitrary unit); activation Q: 0.25; activation time: 27 ms; mass resolution for full scan (MS) (m/z 150 - 1,500): 30,000; mass resolution for data dependent scan (MS^2, MS^3, and MS^4): 7,500; and collision energy: 35 eV.

Supplemental Results

Physicochemical Properties of Momelotinib

Momelotinib (MMB) is a weak base with a $logD_{7.4}$ value 2.4 and pK_a values of 1.4 and 3.7. MMB exhibits pH-dependent aqueous solubility that increases with decreasing pH. The intrinsic solubility is 1.3 µg/mL at pH > 5, and the solubility increases exponentially below pH 3 to 529 µg/mL at pH 0.9. MMB dihydrochloride monohydrate is a physically and chemically stable, non-hydroscopic, crystalline salt form of the drug substance that was selected for clinical development.

Legends for Supplemental Tables

Table S1**.** In vitro study methodology

Table S2. Mean percentage of the [^{14}C]-radioactivity of the most abundant metabolites in pooled human plasma (0-24 h), urine (0-24 h) and feces (0-72 h) and selected metabolites in pooled rat and dog plasma (0-48 h in rat and 0-12 h in dog), urine (0-24 h), bile (0-48 h) and feces (0-48 h)

Table S3. Cumulative recovery of radioactivity following single oral administration of [^{14}C]MMB to intact and BDC Sprague Dawley rats at 15 mg/kg (100 μCi/kg, n = 3) and intact and BDC beagle dogs at 20 mg/kg (10 μCi/kg, n = 3)

Legends for Supplemental Figures

Figure S1. Mass spectra of MMB

Figure S2. Mass spectra of M1

Figure S3. Mass spectra of M5

Figure S4. Mass spectra of M8

Figure S5. Mass spectra of M14

Figure S6. Mass spectra of M16

Figure S7. Mass spectra of M19

Figure S8. Mass spectra of M20

Figure S9. Mass spectra of M21

Figure S10. Mass spectra of M28

Figure S11. Representative radiochromatogram in AUC pooled from (A) rat and (B) dog plasma. Circulating radioactivity above detectable concentrations consisted of MMB (83.4%), M19 (6.9%), and M16 (1.3%) in rat, and MMB (43.4%) and M19 (54.9%) in dog (CPM, counts per minute)

Figure S12. Evidence of closed ring iminium intermediate formation with cyanide trapping experiments: A) Adduct formed with NADPH in human liver microsomes; B) Adduct was not formed without NADPH in human liver microsomes; C) Adduct formed with NADPH with recombinant CYP3A4; D) MS^2 of the CN adduct; E) MS^3 of fragment ion with m/z 357

SUPPLEMENTAL TABLE S1

In vitro study methodology

Lipophilicity ($logD_{7.4}$)

$LogD_{7.4}$ was determined using the octanol/buffer shake flask method (Wenlock et al., 2011). MMB was quantified with an LC-MS/MS method; the MMB LLOQ was 1 ng/mL.

Solubility

The equilibrium solubility of MMB (free base) was determined by adding excess solid to aqueous buffered solutions and agitating for 24 hrs at 25°C. The samples were then centrifuged for 15 min at 13,200 rpm and the supernatants were analyzed by the UPLC-UV (Kerns et al., 2008).

Logarithm of the acid disassociation constant (pKa)

Ionization of the pyrimidine group was estimated to have a pK_a value of approximately 1.4 using an in-silico approach (ACD logD Suite, Version 9). Ionization of the phenylmorpholine group exhibits a pK_a value of 3.7 determined by potentiometric titration.

Permeability

The bidirectional permeability of MMB was assessed in human colonic adenocarcinoma (Caco-2) cell monolayers at two concentrations of 4.15 and 12.45 μg/mL (10 and 30 μM, respectively) using standard methods (Wang et al., 2000).

Blood-to-plasma concentration ratio

MMB was spiked at a nominal concentration of 500 ng/mL (1.2 μM) into whole blood and incubated at 37°C. Whole blood samples sampled at various time points over a 6-hour incubation period were either directly quenched by snap freezing on dry ice or were processed to plasma and then snap frozen. Whole blood or plasma proteins were precipitated using acetonitrile. MMB concentrations in whole blood and plasma were determined by LC-MS/MS.

Protein binding

Protein binding of MMB and its metabolites M19 and M21 was assessed in pooled plasma from Sprague-Dawley rats, beagle dogs, and humans (Kariv et al., 2001), as well as in human hepatic microsomes (Obach, 1997). Protein binding of MMB and M21 was also assessed in 1% fetal calf serum and 10% fetal calf serum in eagle's minimum essential medium. Analyte concentrations were quantified using an LC-MS/MS.

Hepatocyte stability

MMB (0.21 μg/mL; 0.5 μM) was incubated in cryopreserved hepatocytes from rats, dogs, and humans (0.4–1.0 million cells/mL) over 1.5 hours (Obach, 1999). The metabolic stability of M21 (0.43 μg/mL; 1 μM) was assessed in cryopreserved human hepatocytes (1.0 million cells/mL). The hepatic extraction ratio (E_H), defined as the ratio of the predicted clearance (CL) over the hepatic blood flow (Q_h), was categorized as low (< 0.3), intermediate (0.3–0.7), high (0.7–0.95), or very high (>0.95).

Enzymology

The rates of MMB (0.83 μg/mL; 2 μM) metabolic conversion and formation of M21 were determined in the presence or absence of the pan-cytochrome P450 (CYP) inhibitor 1-aminobenzotriazole (ABT) (Emoto et al., 2003) and the aldehyde oxidase inhibitor hydralazine (Strelevitz et al., 2012). The relative contribution of individual CYP enzymes to MMB metabolism was also determined. MMB was incubated for up to 6 hours with the human recombinant CYP isoforms (1A2, 2A6, 2B6, 2C9, 2C19, 2D6, 2E1, 3A4, and 3A5), and NADPH (Chen et al., 2011; Crespi and Penman, 1997). MMB and M21 concentrations were determined by LC-MS/MS.

The rates of MMB (0.83 μg/mL; 2 μM) metabolic conversion and formation of M21 were also determined in the presence or absence of the mechanism-based inhibitor ritonavir (RTV; 3 μM) and the aldehyde oxidase inhibitor raloxifene (3 μM). The relative contribution of RTV and raloxifene to MMB metabolism and M21 formation was determined. MMB was incubated for up to 6 hours with the human hepatocytes (1 million cells). MMB and M21 concentrations were determined by LC-MS/MS.

The formation of an iminium intermediate by MMB was supported by a cyanide trapping experiment in human liver microsomes (100 pmol/mL) containing 0.5 mg/mL reductase protein in the presence or absence of NADPH and in comparison to that with recombinant CYP3A4 in the presence of NAPDH. The incubation time was 0 and 70 minutes. Potassium cyanide (5 mM) was used to trap the potential reactive iminium intermediate. The CN adduct formation was determined by LC-HRMS/MS.

SUPPLEMENTAL TABLE S2

Mean percentage of the [^{14}C]-radioactivity of the most abundant metabolites in pooled human plasma (0-24 h), urine (0-24 h) and feces (0-72 h) and selected metabolites in pooled rat and dog plasma (0-48 h in rat and 0-12 h in dog), urine (0-24 h), bile (0-48 h) and feces (0-48 h)

Metabolites			Human		Intact rat		BDC rat	Intact dog		BDC dog
			P	U / F	P	U / F	U / B / F	P	U / F	U / B / F
ID	Accurate MH$^+$	Δppm	% of [^{14}C] AUC	% of DRM	% of [^{14}C] AUC	% of DRM	% of DRM	% of [^{14}C] AUC	% of DRM	% of DRM
MMB	415.1876	-0.2	17.3	0.6 / 12.6	83.4	0.1 / 17.8	0.2 / 0.3 / 28.2	43.4	5.4 / 20.1	ND / 2.4 / 25.5
M21	429.1663	-1.6	64.2	11.5 / 12.7	ND	0.1 / 0.6	0.6 / 0.1 / 0.4	ND	ND / ND	ND / ND / ND
M8	447.1768	-1.3	5.8	0.7 / 2.5	ND	ND / ND	ND / ND / ND	ND	ND / ND	ND / ND / ND
M19	377.1604	-1.1	5.2	ND / 7.1[a]	6.9	0.4 / 6.2	0.3 / 1.7 / 1.1	54.9	0.3 / 15.9	19.9 / 9.0 / 10.4
M5	461.1564	-0.9	2.7	2.3 / 3.8	ND	ND / ND	ND / ND /ND	ND	ND / ND	ND / ND / ND
M28	391.1398	-0.8	2.5	1.0 / ND	ND	ND / ND	ND / ND/ ND	ND	ND / ND	ND / ND / ND
M20	387.1565	+0.3	2.3	ND / 1.7	ND	0.3 / 1.3	0.6 / 0.2 / 0.4	ND	ND / ND	ND / ND / ND
M14[d]	390.1554	-1.8	ND	1.8 / 21.4	ND	ND / ND	ND / ND /ND	ND	ND / ND	ND / ND / ND
M16[e]	389.1713	-2.1	ND	1.6 / 1.5	1.3	1.8 / 5.8	2.1 / 2.2[b] / 0.9	ND	ND / 3.0	17.7 / 6.8 / 0.9

M1[f]	591.2188	-1.7	ND	1.5[c] / ND	ND	ND / ND	ND / ND / ND	ND	ND / ND	ND / ND / ND

[a] M19 co-elute with M33 (m/z = 431.1469, oxidative metabolite) in human feces.
[b] M16 co-eluted with the oxidation plus glucuronidation of MMB with m/z = 607.2145 in rat bile.
[c] M1 co-eluted with the oxidation plus glucuronidation of M21 with m/z = 621.1921 in human urine.
[d] M14 was listed because it was a major metabolite in human feces.
[e] M16 was listed because it represented >10% of the DRM in bile duct-cannulated dog urine.
[f] M1 was listed because it represented a phase II metabolism pathway in human in Figure 2.
MH^+, protonated molecular ion; Δppm, mass accuracy expressed in parts per million.
BDC, bile duct-cannulated; B, bile; DRM = drug-related materials; F, feces; G, glutathione; ND, not detected; P, plasma; U, urine.

SUPPLEMENTAL TABLE S3

Cumulative recovery of radioactivity following single oral administration of [^{14}C]MMB to intact and BDC Sprague Dawley rats at 15 mg/kg (100 μCi/kg, n = 3) and intact and BDC beagle dogs at 20 mg/kg (10 μCi/kg, n = 3)

		Cumulative recovery of radioactivity, % DRM (Mean ± SD)				
Species	**Collection time duration, h**	**Urine**	**Feces**	**Bile**	**Carcass (residual)**	**Total excreta[a]**
Intact rat	0–24	13.2 ± 1.7	62.6 ± 6.6	NA	0.3 ± 0.1	NA
	0–48	13.9 ± 1.8	75.1 ± 3.4	NA	0.4 ± 0.1	NA
	0–168	14.1 ± 1.8	77.2 ± 3.3	NA	4.8 ± 0.8	96.1 ± 0.8
BDC rat	0–24	15.2 ± 2.9	36.9 ± 12.3	29.2 ± 2.2	0.3 ± 0.2	NA
	0–48	16.2 ± 3.5	42.9 ± 8.7	31.7 ± 3.4	0.4 ± 0.2	NA
	0–168	16.6 ± 3.7	44.3 ± 8.0	33.0 ± 3.9	2.9 ± 0.7	96.8 ± 0.6

	0–24	9.0 ± 5.2	45.9 ± 31.8	NA	1.0 ± 0.9	NA
Intact dog	0–48	9.3 ± 5.2	69.7 ± 5.4	NA	1.3 ± 1.2	NA
	0–168	9.6 ± 5.1	70.8 ± 5.3	NA	10.7 ± 2.4	91.2 ± 2.5
	0–24	2.4 ± 1.1	45.2 ± 4.0	40.4 ± 6.5	0.7 ± 0.6	NA
BDC dog	0–48	2.6 ± 1.1	47.3 ± 4.6	41.3 ± 6.3	0.9 ± 0.7	NA
	0–168	2.8 ± 1.2	47.5 ± 4.5	41.5 ± 6.3	2.7 ± 2.9	94.4 ± 1.2

[a] Total recovery of radioactivity in excreta includes cage rinses, cage wash, cage wipe, bile cannula rinse, and jacket rinse.

BDC, bile duct-cannulated; DRM = drug-related materials; NA, not applicable; SD, standard deviation.

Supplemental Figures

Figure S1. Mass spectra of MMB. The mass spectra had a retention time and fragmentation pattern corresponding to the synthetic reference standard of MMB.

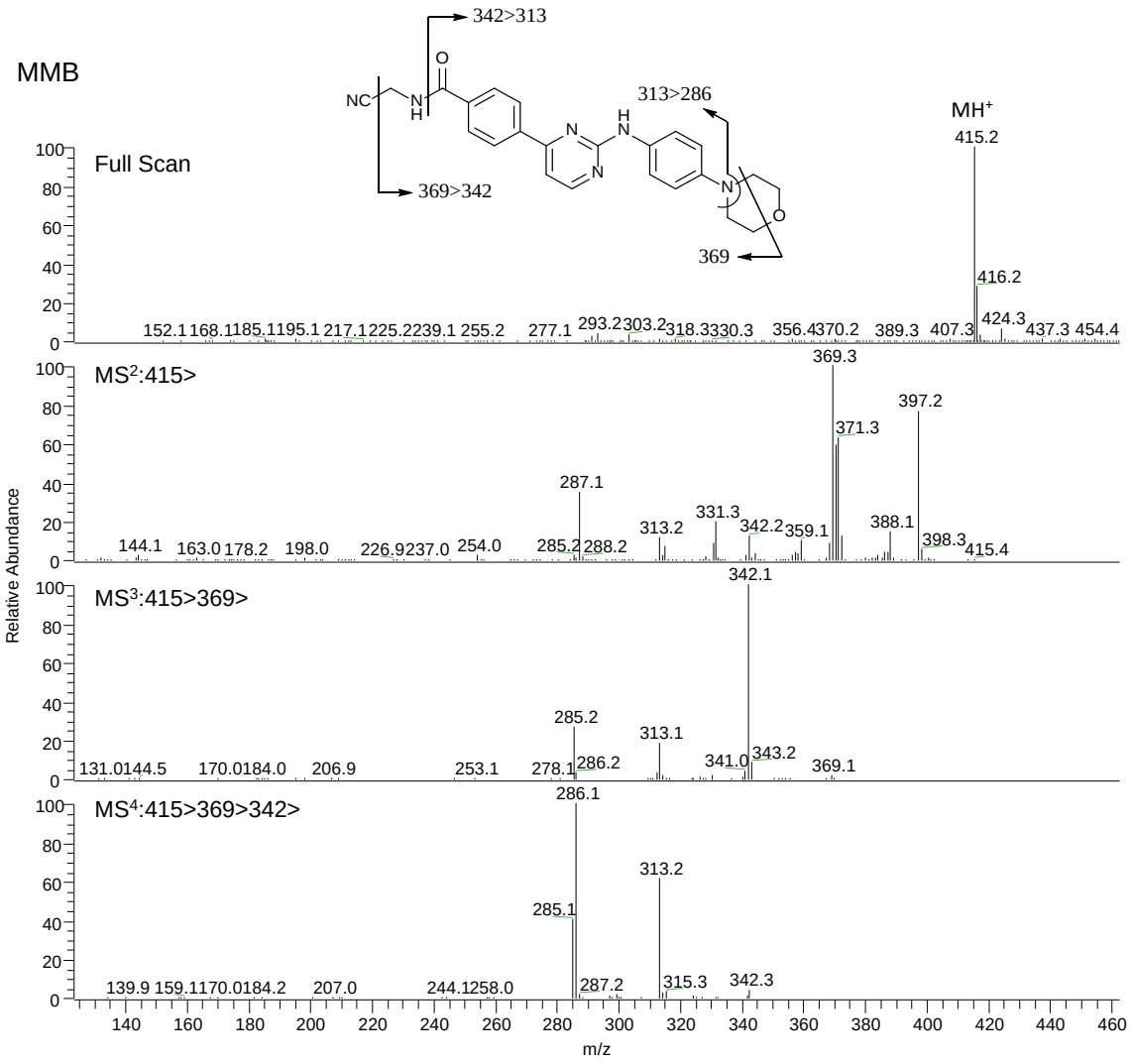

Figure S2. Mass spectra of M1. The protonated molecular ion of M1 was observed at *m/z* 591.2188, which is consistent with the elemental composition of a glucuronide conjugate of MMB. The diagnostic neutral loss of 176 Da, typical of glucuronide conjugates, leading to an ion at *m/z* 415 (aglycone) in the MS^2 spectrum supported the structural assignment. The exact position of conjugation could not be determined from the mass spectral data.

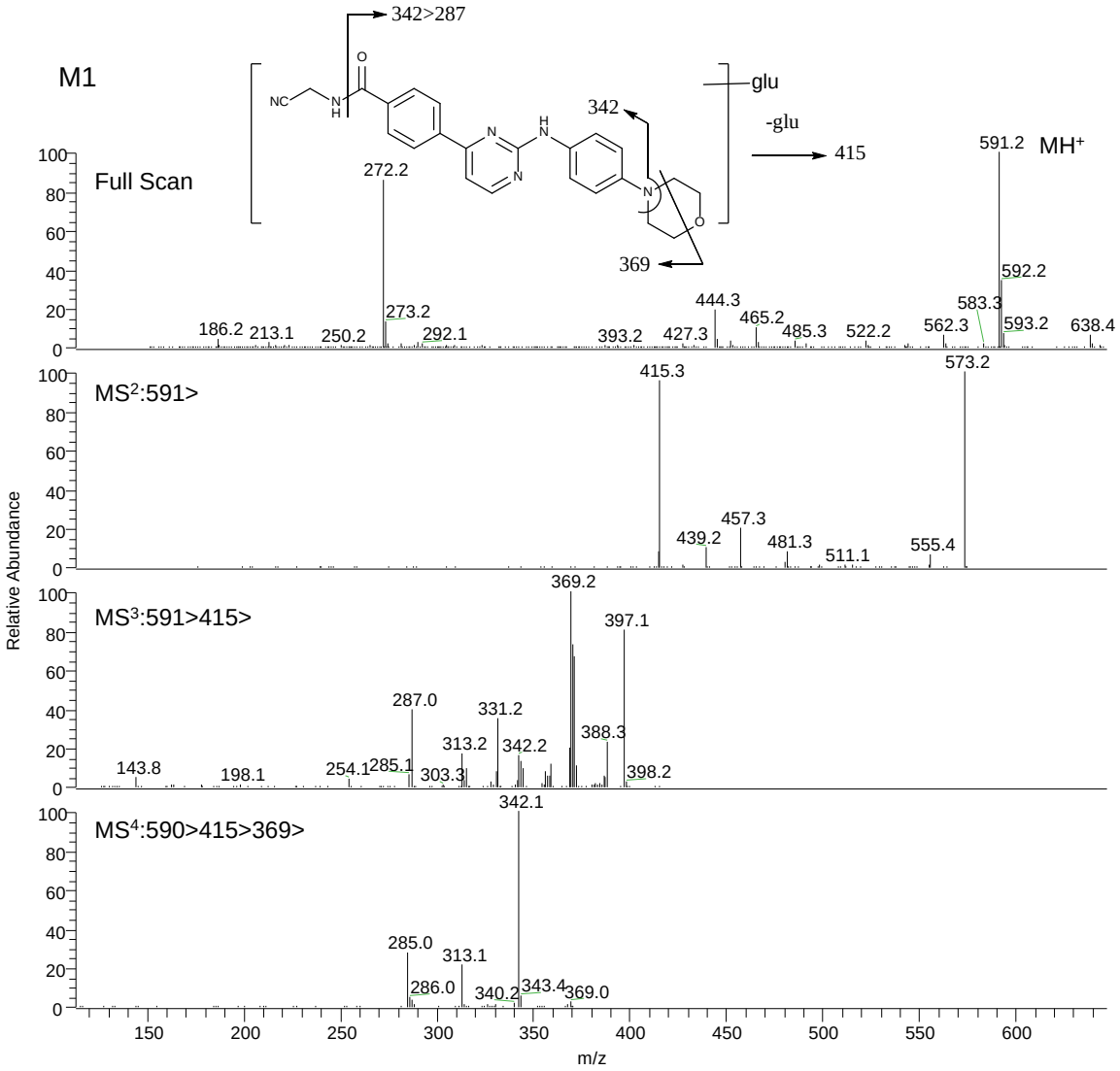

Figure S3. Mass spectra of M5. The protonated molecular ion of M5 was observed at *m/z* 461.1564, which is consistent with the elemental composition of a dihydroxylated analogue of M21 (calculated value of 461.1568). MS/MS fragmentation of ions at *m/z* 417 and 361 suggested the possible opening of the morpholine ring with the formation of carboxylic acid. The characteristic loss of 46 amu (HCOOH) from *m/z* 361 to produce an ion at *m/z* 315 supports the possible ring cleavage of morpholine moiety. The mass spectra and the proposed fragmentation pathways are shown here.

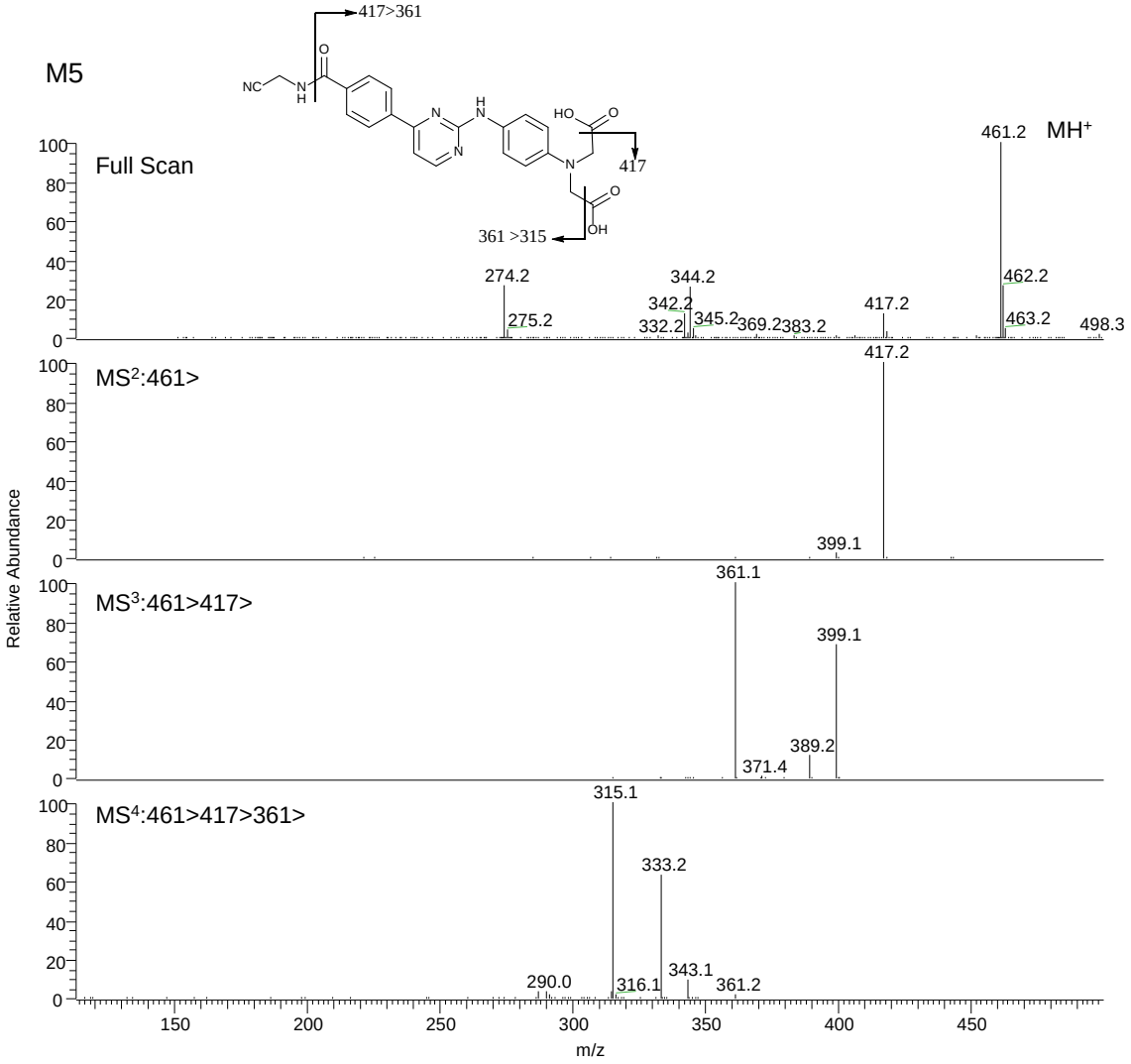

Figure S4. Mass spectra of M8. The mass spectra had a retention time and fragmentation pattern corresponding to the synthetic reference standard of M8.

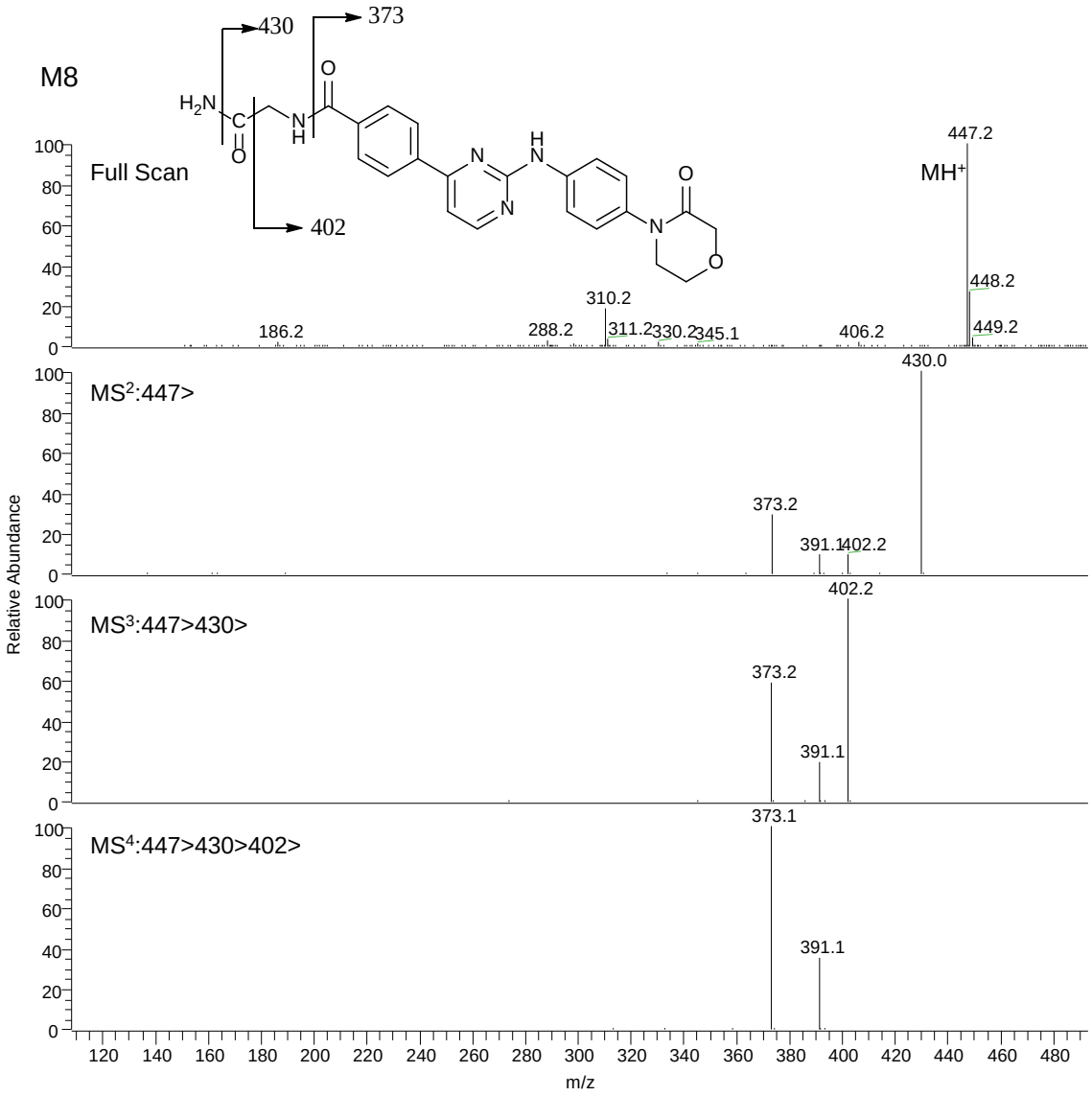

Figure S5. Mass spectra of M14. The protonated molecular ion of M14 was measured by Orbitrap at *m/z* 391.1398, which is consistent with the elemental composition of a morpholine oxidized analogue of M19 (calculated value of 391.1401). The mass spectral fragmentation pattern showed ions with an increment of 14 amu (representing an addition of a keto functional group) to all the ions observed in the spectrum of M19. The mass spectral fragmentation patterns are consistent with the proposed structure. The mass spectra and the proposed fragmentation pathways are shown here.

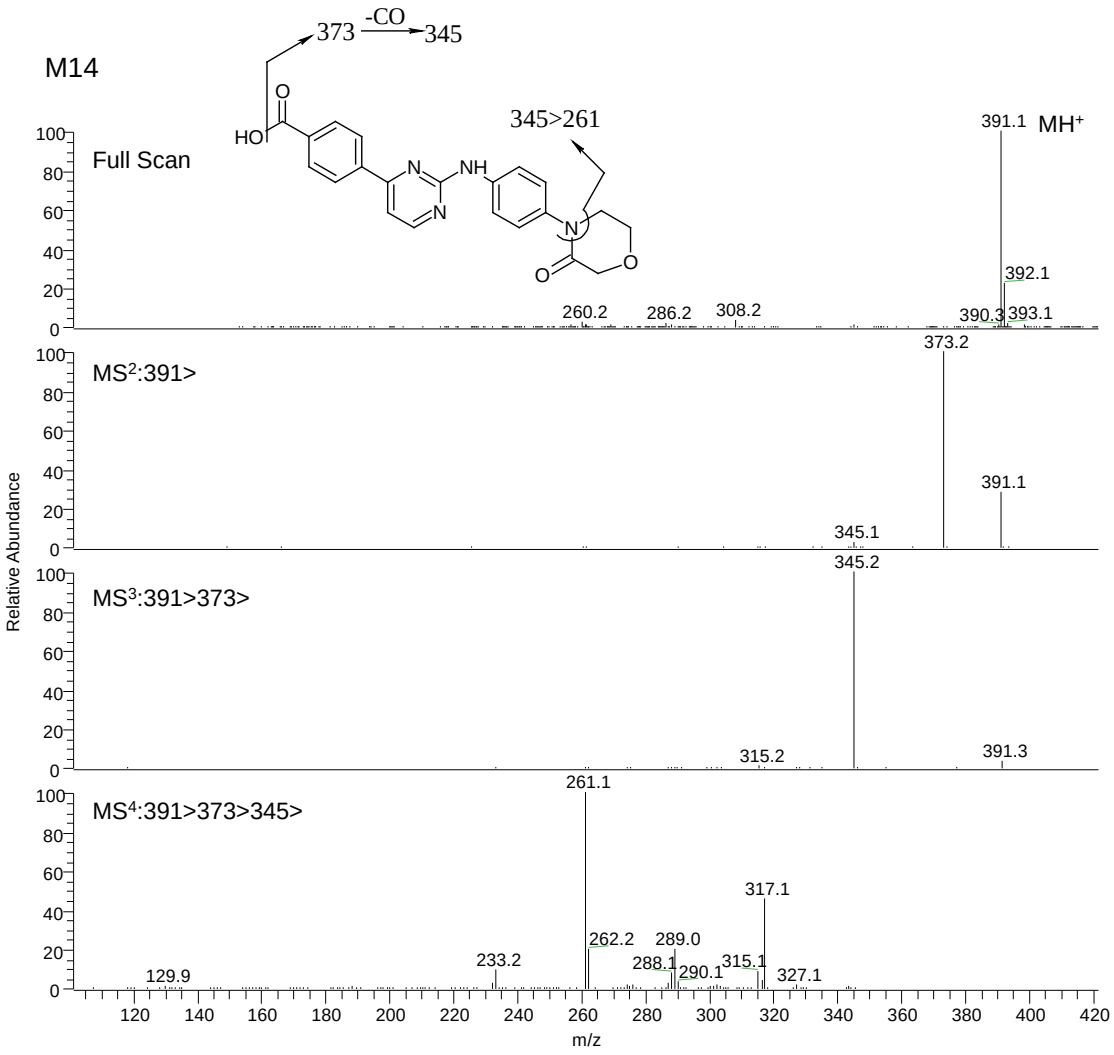

Figure S6. Mass spectra of M16. The protonated molecular ion of M16 was observed at *m/z* 389.1713, which is consistent with the elemental composition of a morpholine ring-opened analogue of MMB (calculated value of 389.1721). This metabolite is proposed to be formed after the dealkylation of morpholine where an ethylene (CH_2=CH_2) moiety is lost (-28 amu) from MMB. The mass spectral fragmentation patterns supported this structural assignment. MS/MS of ion at *m/z* 389 produced ions at *m/z* 371 (-18 amu, loss of H_2O) and 344 (-45 amu, loss of ethanol), hence supporting the assigned structure. The mass spectra and the proposed fragmentation pathways are shown here.

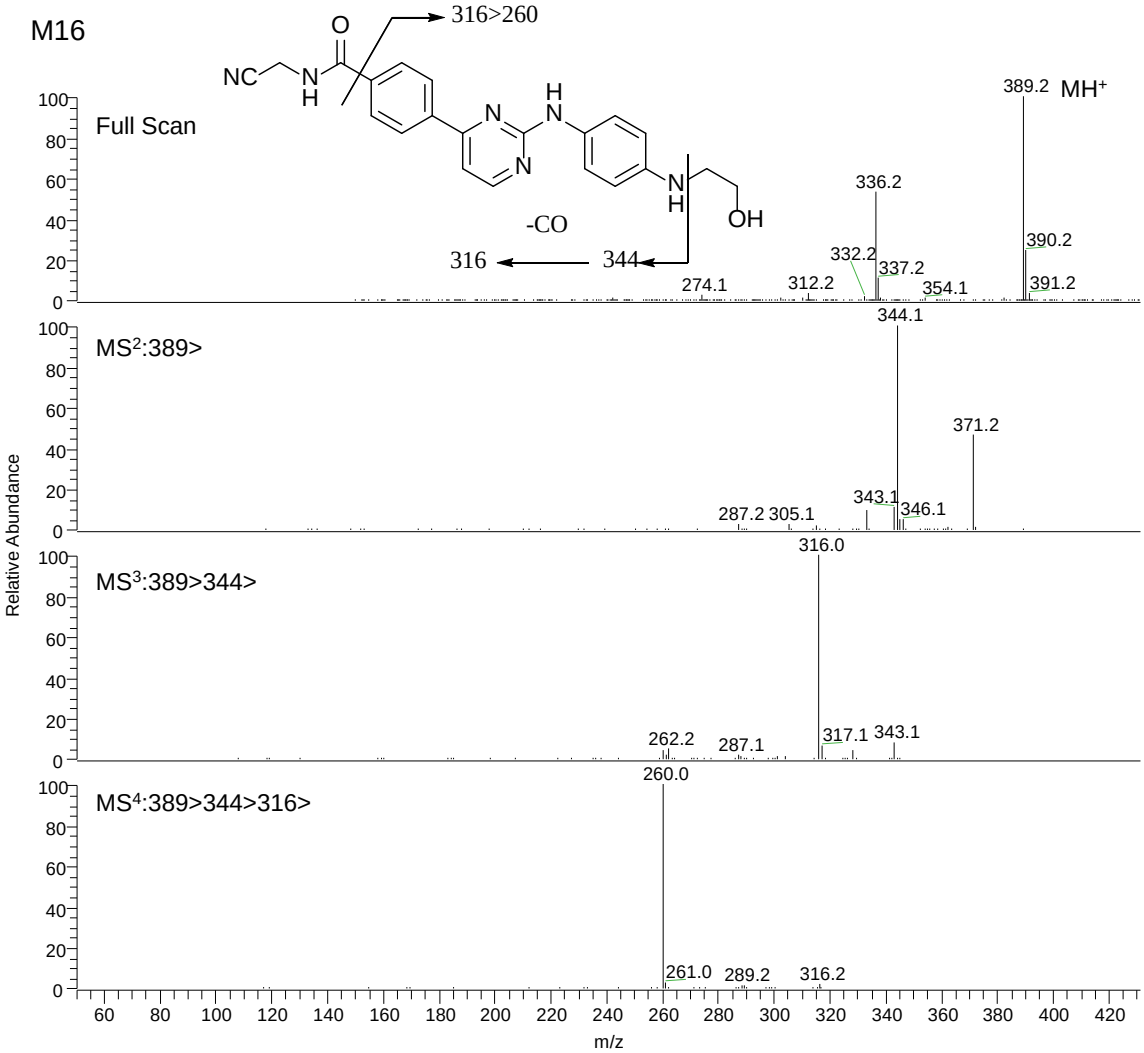

Figure S7. Mass spectra of M19. The protonated molecular ion of M19 was observed at *m/z* 377.1604, which is consistent with the elemental composition of an amide hydrolyzed analogue of MMB (calculated m/z value of 377.1610). The structure of M19 was confirmed by comparison with synthetic standard. The mass spectra and the proposed fragmentation pathways are shown here.

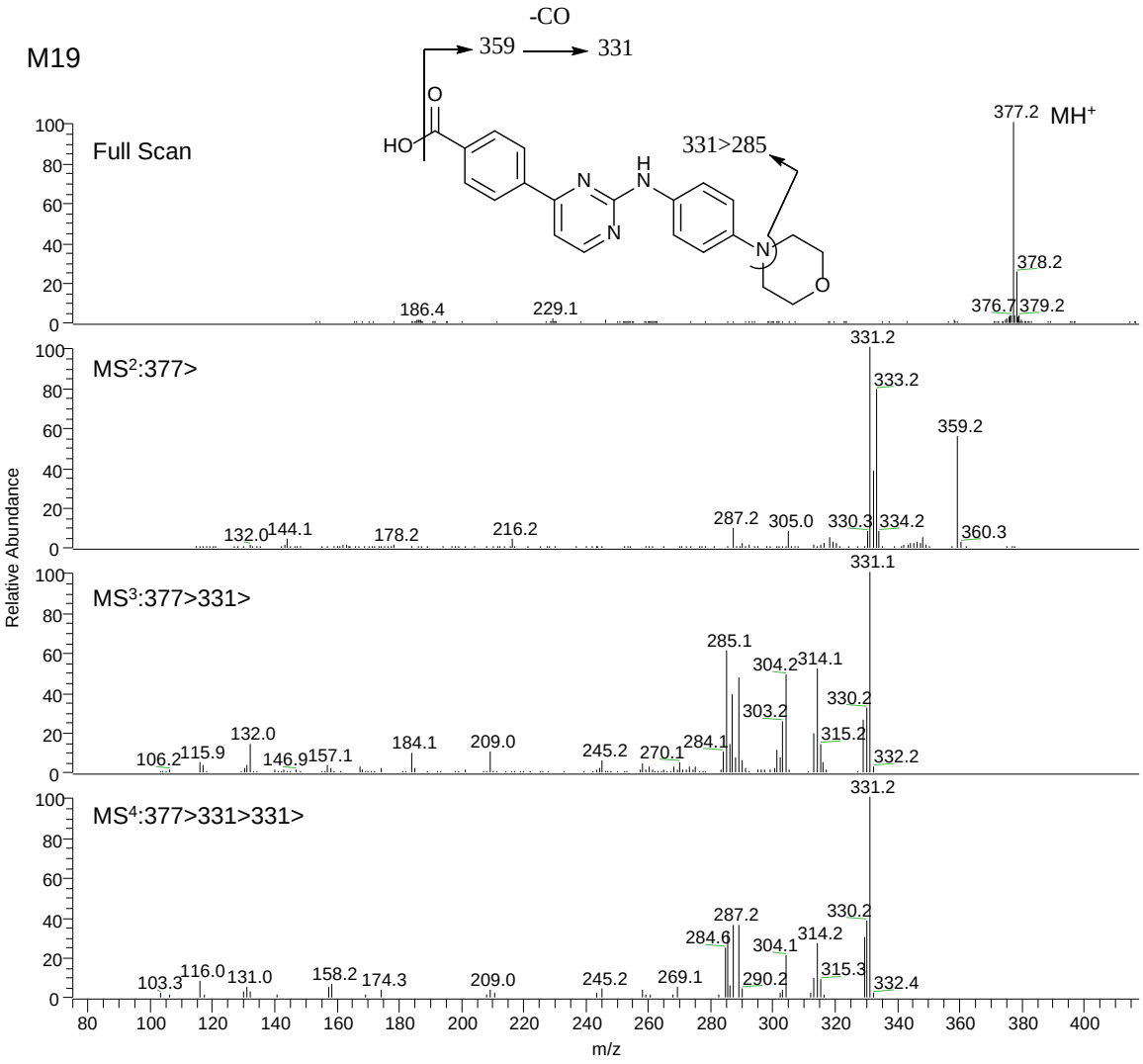

Figure S8. Mass spectra of M20. The protonated molecular ion of M20 was observed at *m/z* 387.1565, which is consistent with the elemental composition of a morpholine ring-cleaved/acetylated analogue of MMB (calculated m/z value of 387.1564). MS/MS of ion at *m/z* 387 produced a typical loss of 56 amu (cyanomethylamide moiety), resulting in an ion at *m/z* 331 which subsequently was fragmented to produce base ion at *m/z* 303 (- 28 amu, loss of CO). The mass spectral fragmentation pattern was consistent with the proposed structure. The mass spectra and the proposed fragmentation pathways are shown here.

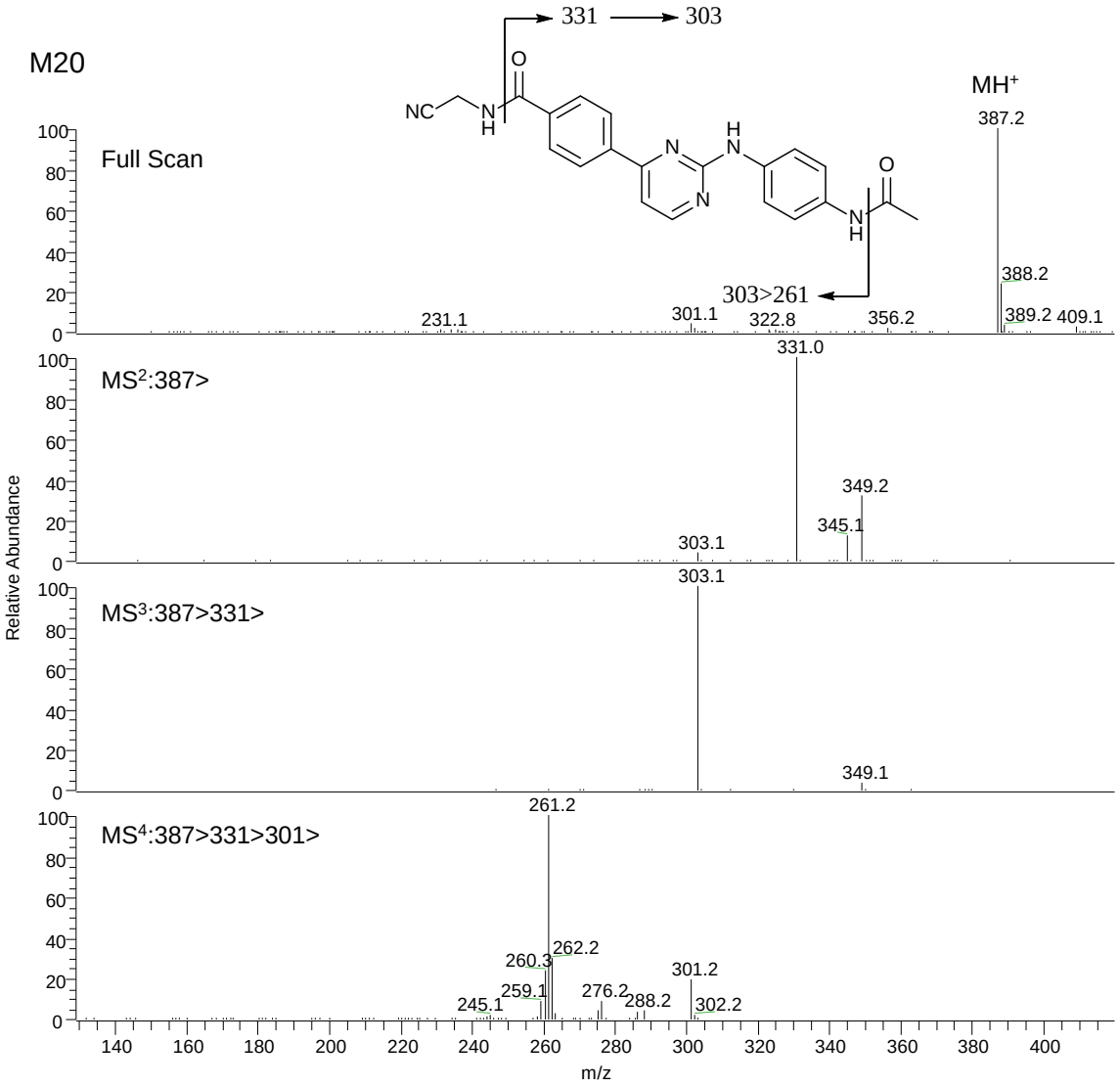

Figure S9. Mass spectra of M21. The protonated molecular ion of M21 was observed at *m/z* 429.1663, which is consistent with the elemental composition of a keto analogue of MMB (calculated value of 429.1670). The structure of M21 was confirmed by comparison with synthetic standard. The mass spectra and the proposed fragmentation pathways are shown here.

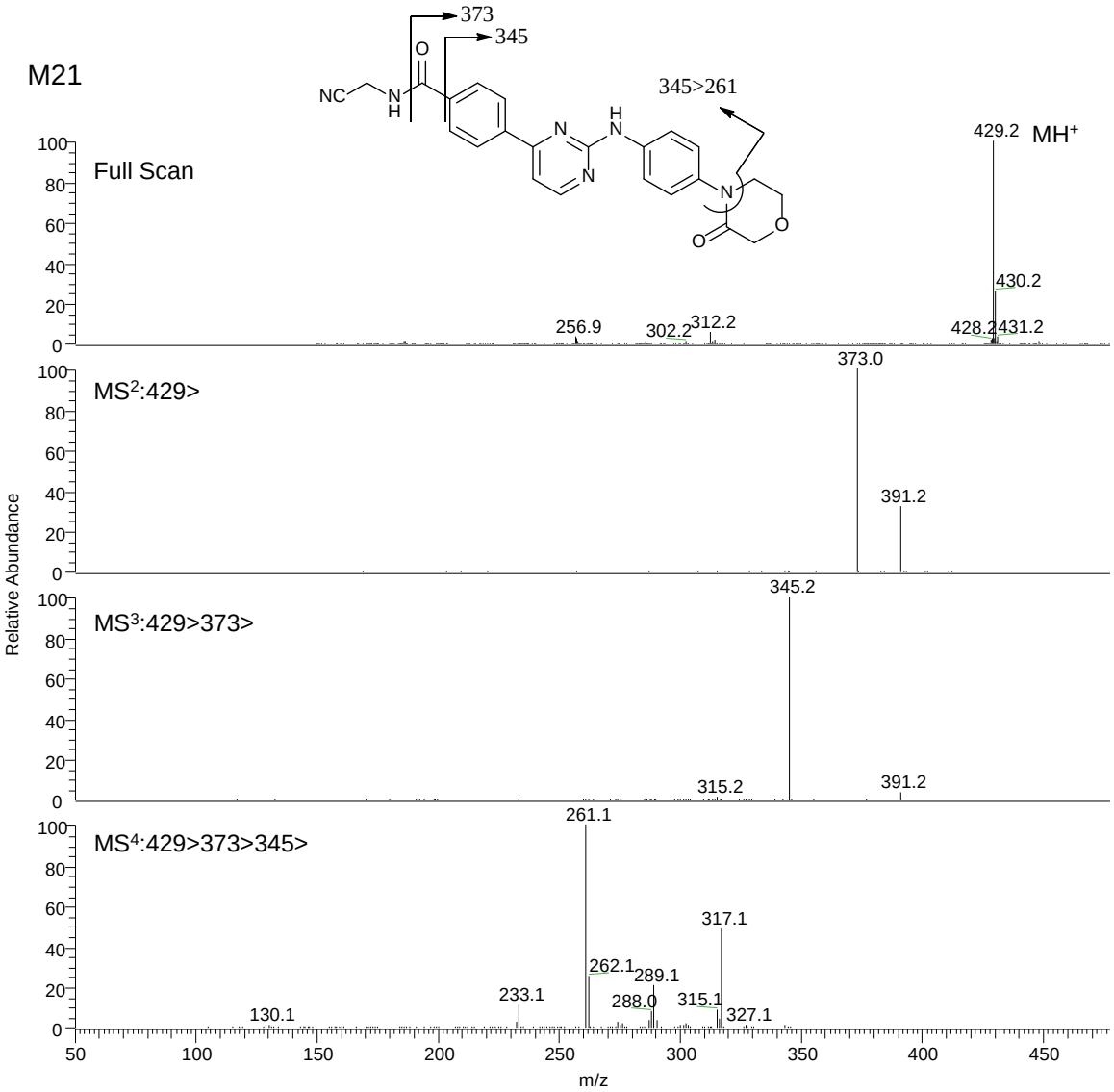

Figure S10. Mass spectra of M28. The protonated molecular ion of M28 was observed at m/z 390.1554, which is consistent with the elemental composition of an N-dealkylated analogue of M21 (calculated m/z value of 390.1561). The MS/MS of ion at m/z 390 produced a fragment ion at m/z 373 (-17 amu, loss of NH3) which was further fragmented to produce ion at m/z 345 (- 28 amu, loss of CO). Further MS/MS of ion at m/z 345 produced fragment ions consistent with what was observed in the mass spectra of M21 (see **Figure S9**). Hence, the structure of M28 is proposed to be the N-dealkylated analogue of M21. The mass spectra and the proposed fragmentation pathways are shown here.

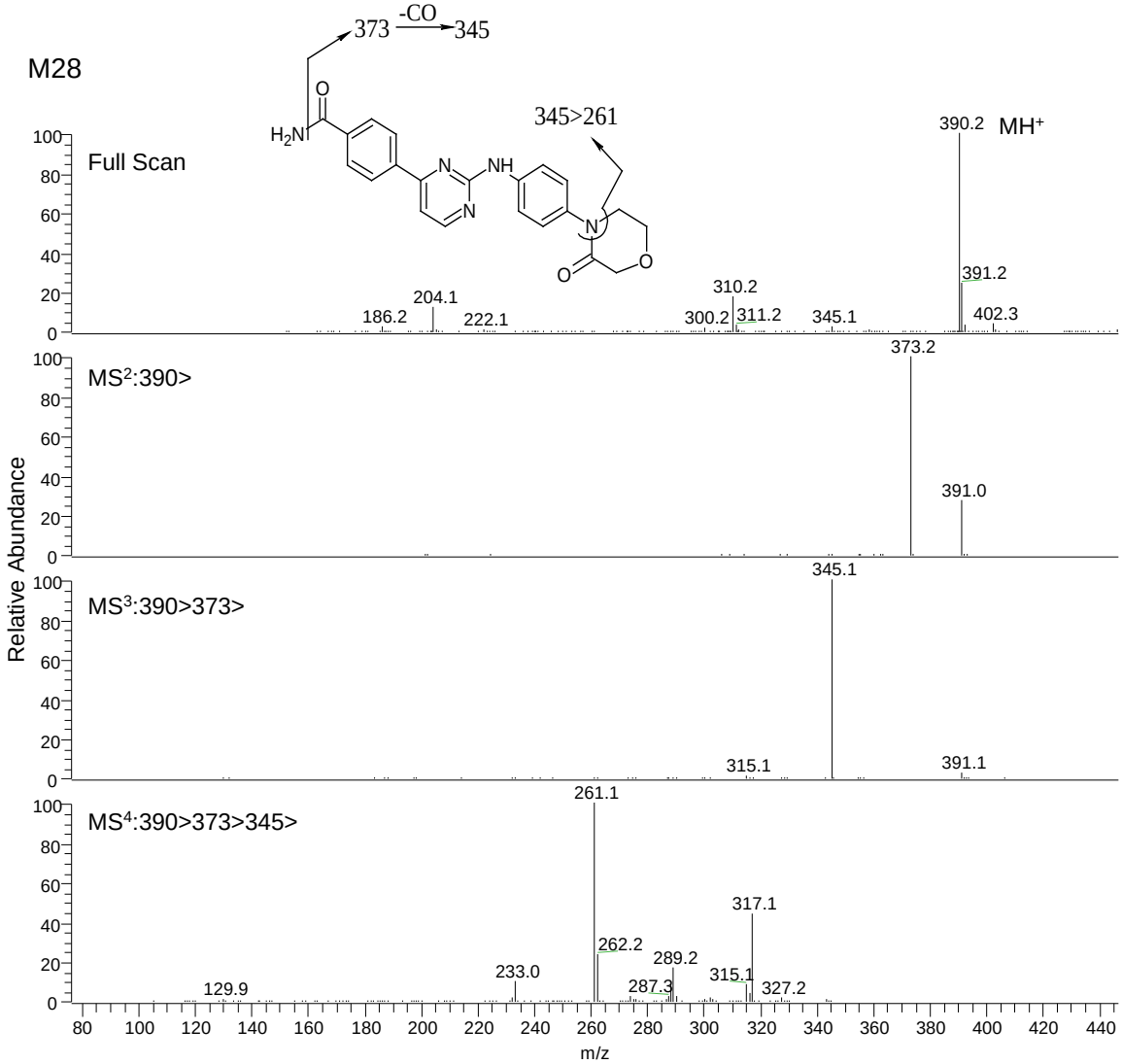

Figure S11. Representative radiochromatogram in AUC pooled from (A) rat and (B) dog plasma. Circulating radioactivity above detectable concentrations consisted of MMB (83.4%), M19 (6.9%), and M16 (1.3%) in rat, and MMB (43.4%) and M19 (54.9%) in dog (CPM = counts per minute).

A

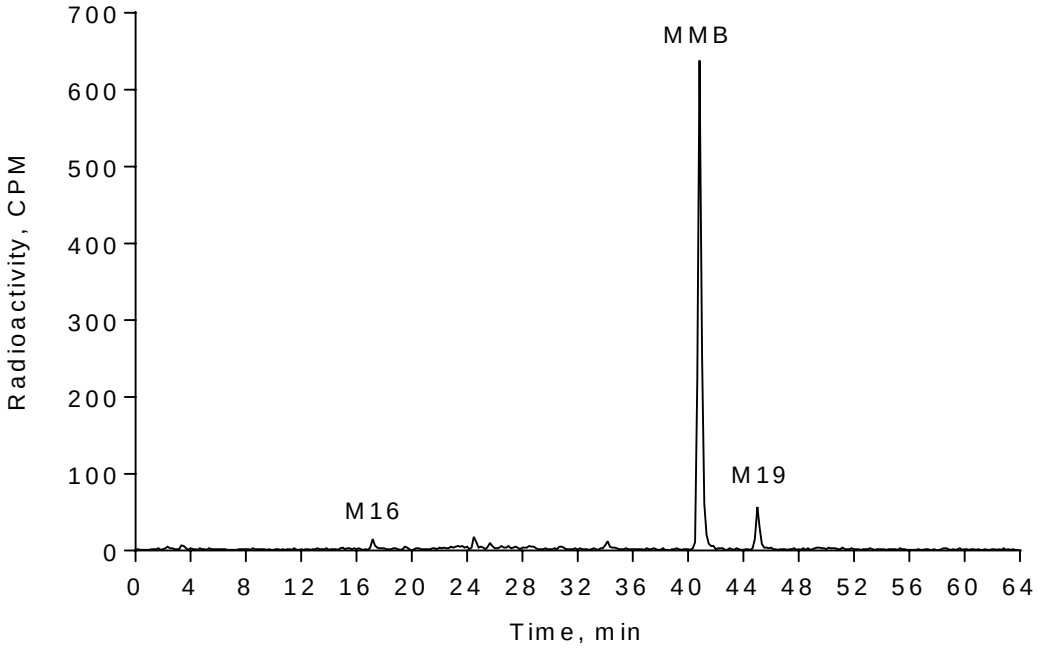

B

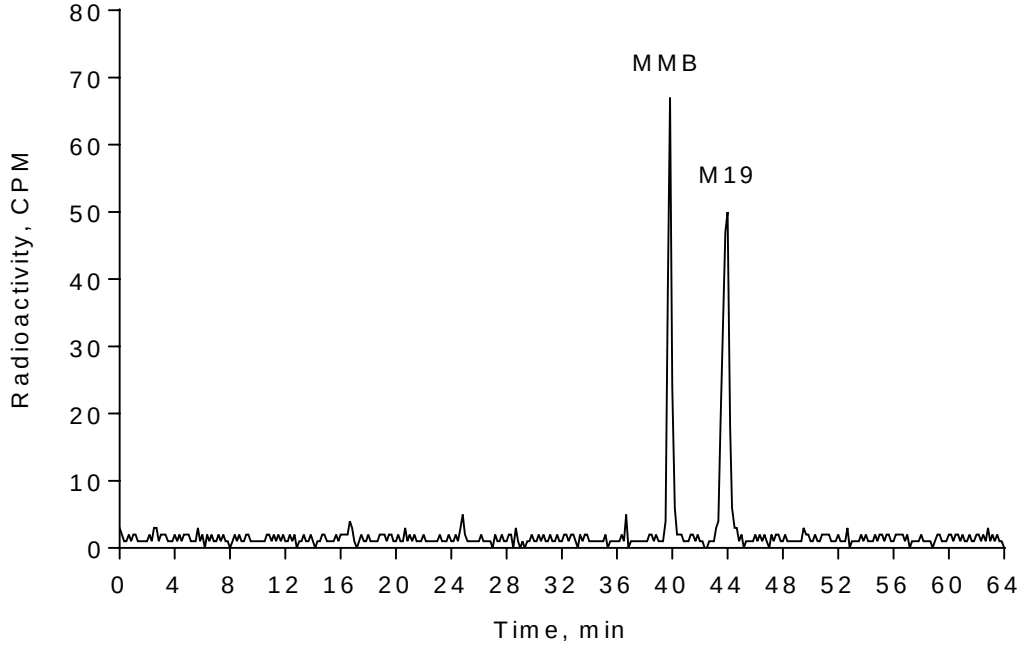

Figure S12. Evidence of closed ring iminium intermediate formation with cyanide trapping experiments: A) Adduct formed with NADPH in human liver microsomes; B) Adduct was not formed without NADPH in human liver microsomes; C) Adduct formed with NADPH with recombinant CYP3A4; D) MS^2 of the CN adduct; E) MS^3 of fragment ion with m/z 357.

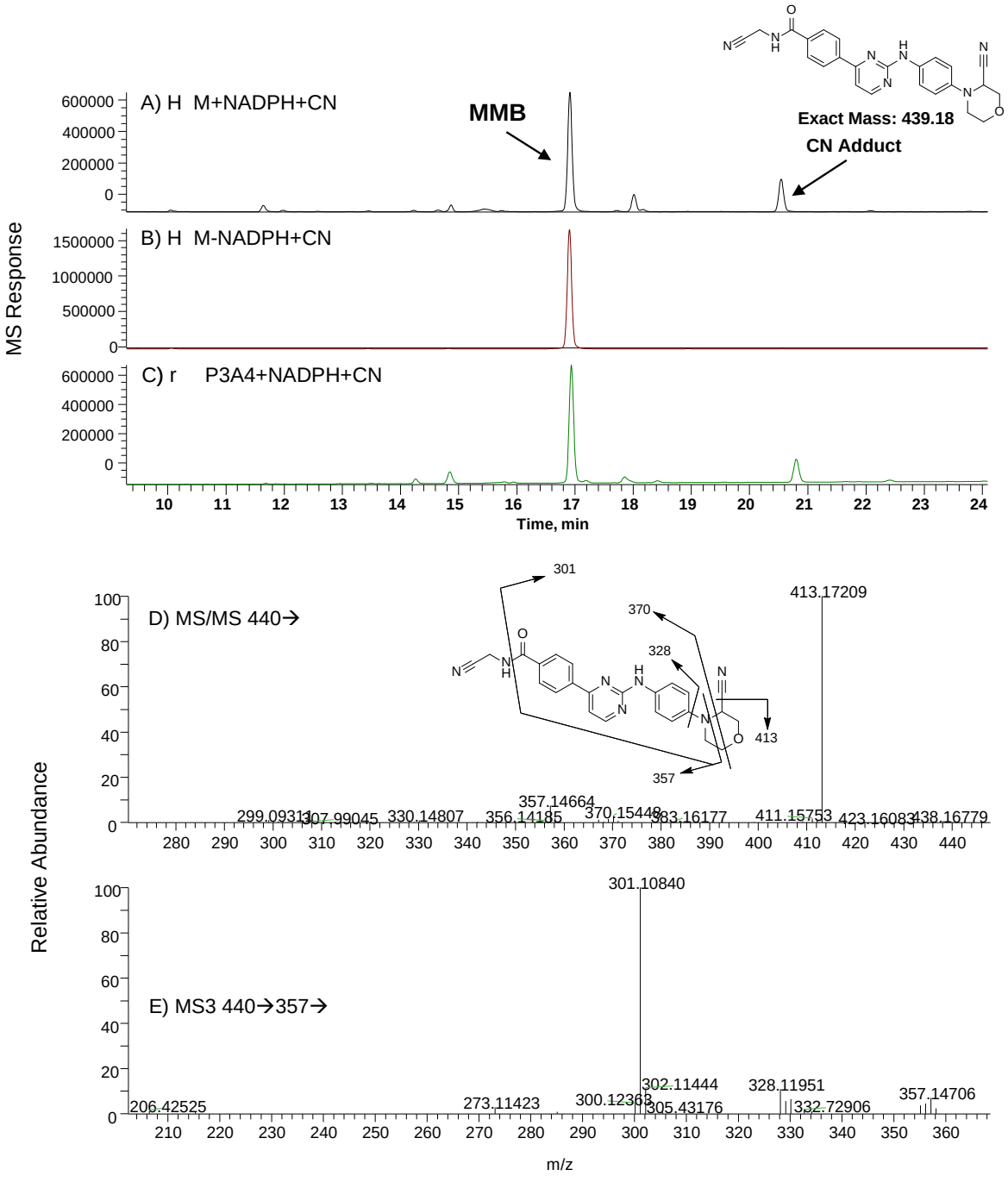

Supplemental References:

Chen Y, Liu L, Nguyen K, and Fretland AJ (2011) Utility of intersystem extrapolation factors in early reaction phenotyping and the quantitative extrapolation of human liver microsomal intrinsic clearance using recombinant cytochromes P450. *Drug Metab Dispos* **39**:373-382.

Crespi CL and Penman BW (1997) Use of cDNA-expressed human cytochrome P450 enzymes to study potential drug-drug interactions. *Adv Pharmacol* **43**:171-188.

Emoto C, Murase S, Sawada Y, Jones BC, and Iwasaki K (2003) In vitro inhibitory effect of 1-aminobenzotriazole on drug oxidations catalyzed by human cytochrome P450 enzymes: a comparison with SKF-525A and ketoconazole. *Drug Metab Pharmacokinet* **18**:287-295.

Kariv I, Cao H, and Oldenburg KR (2001) Development of a high throughput equilibrium dialysis method. *J Pharm Sci* **90**:580-587.

Kerns EH, Di L, and Carter GT (2008) In vitro solubility assays in drug discovery. *Curr Drug Metab* **9**:879-885.

Obach RS (1997) Nonspecific binding to microsomes: impact on scale-up of in vitro intrinsic clearance to hepatic clearance as assessed through examination of warfarin, imipramine, and propranolol. *Drug Metab Dispos* **25**:1359-1369.

Obach RS (1999) Prediction of human clearance of twenty-nine drugs from hepatic microsomal intrinsic clearance data: an examination of in vitro half-life approach and nonspecific binding to microsomes. *Drug Metab Dispos* **27**:1350-1359.

Strelevitz TJ, Orozco CC, and Obach RS (2012) Hydralazine as a selective probe inactivator of aldehyde oxidase in human hepatocytes: estimation of the contribution of aldehyde oxidase to metabolic clearance. *Drug Metab Dispos* **40**:1441-1448.

Wang Z, Hop CECA, Leung KH, and Pang JM (2000) Determination of in vitro permeability of drug candidates through a Caco-2 cell monolayer by liquid chromatography/tandem mass spectrometry. *J Mass Spectrom* **35**:71-76.

Wenlock MC, Potter T, Barton P, and Austin RP (2011) A method for measuring the lipophilicity of compounds in mixtures of 10. *J Biomol Screening* **16**:348-355.